Biosensors and Bioelectronics 140 (2019) 111350

Contents lists available at ScienceDirect

Biosensors and Bioelectronics

journal homepage: www.elsevier.com/locate/bios

Fiber optic surface plasmon resonance biosensor for detection of PDGF-BB in serum based on self-assembled aptamer and antifouling peptide monolayer

Husun Qian[a,1], Yu Huang[b,1], Xiaolei Duan[a], Xiaotong Wei[a], Yunpeng Fan[a], Delu Gan[a], Shujun Yue[a], Wei Cheng[c], Tingmei Chen[a,*]

[a] Key Laboratory of Clinical Laboratory Diagnostics (Ministry of Education), College of Laboratory Medicine, Chongqing Medical University, Chongqing, 400016, PR China
[b] Chongqing Institute of Green and Intelligent Technology, Chinese Academy of Sciences, Chongqing, 400714, PR China
[c] The Center for Clinical Molecular Medical Detection, The First Affiliated Hospital of Chongqing Medical University, Chongqing, 400016, China

ARTICLE INFO

Keywords:
Fiber optic
Surface plasmon resonance
Biosensor
PDGF-BB
Antifouling peptide

ABSTRACT

Herein, a home-build fiber optic surface plasmon resonance (FO-SPR) biosensing platform has been developed for highly sensitive detection of platelet-derived growth factor (PDGF-BB) based aptamer-functionalized AuNPs for signal enhancement. In this biosensor, the PDGF-BB aptamer was used to specifically capture PDGF-BB, and the antifouling peptide demonstrated great ability for resisting non-specific adsorption. After a sandwich reaction, the aptamer, PDGF-BB and aptamer-functionalized AuNPs complexes were formed on the fiber optic (FO) probe surface to significantly amplify FO-SPR signal. This method exhibited a broad detection range from 1 to 1000 pM of PDGF-BB and a low detection limit of 0.35 pM. Moreover, this biosensor was successfully applied to the detection of PDGF-BB in 10% human serum samples without suffering from serious interference owing to the excellent antifouling property of the peptide. Thus, this developed FO-SPR biosensor could be a potential alternative device for proteins determination, even as a point-of-care diagnostic tool (POCT) in clinical application.

1. Introduction

Platelet-derived growth factor (PDGF-BB), separated from platelets, can act as a significant biomarker of tumor early diagnosis, metastasis and recurrence. (Yi et al., 2002; Zhang et al., 2015). In normal cells, the expression of PDGF-BB is maintained at a low or undetectable level (Kim et al., 2015). In contrast, PDGF-BB is mostly oversecreted in numerous type of cancers, such as sarcomas and gliboblastomas (Hosaka et al., 2013). Thus, designing an accurate and sensitive method to measure target protein is crucial for early clinical diagnostics and biomedical research.

Up to now, most of strategies have been proposed to detect PDGF-BB, such as electrochemistry (Jiang et al., 2017), colorimetry (Zou et al., 2017), chemiluminescence (Bi et al., 2014), fluorescence (Bahreyni et al., 2019), and surface-enhanced Raman spectroscopy (Ye et al., 2016). Although most of these traditional methods achieve highly sensitive detection of PDGF-BB, relatively sophisticated instrumentations, expensive reagents and complicated procedures are often needed, which limit their application in the clinical diagnosis. Therefore, the simple and cost-effective biosensing methods for sensitive determination of PDGF-BB still remains an urgent need.

Due to the unique properties of simple synthesis, good stability and flexibility in labeling, aptamers have been widely used as the recognition probes to provide a strong affinity and specificity for biomolecule assay (Meng et al., 2016). During the past few years, aptamer-based biosensors (aptasensors) for PDGF-BB detection have made great improvements in medical diagnosis (Razmi et al., 2018). The analytical performance of aptasensors to assay PDGF-BB strongly depends on the specific bioaffinity between aptamer and its designated target. For instance, Bahreyni et al. (2019) developed a PDGF-BB aptasensor with enhanced analytical performance by using dsDNA and magnetic beads signal amplification strategy. Song et al. (2014) designed a highly sensitive PDGF-BB electrochemical aptasensor array by sandwich-type reaction to form complexes for signal amplification. Wang et al. (2018b) proposed a PDGF-BB electrochemical aptasensor based on cascade cycle signal enlargement initiated by nucleic acid aptamers. However, the practical application of aptasensors faces a great challenge in complex biological media. The complex biological media significantly not only impairs the analytical performance of biosensor but also bring severe background interference for sensing, resulting in a

* Corresponding author.
E-mail address: tingmeichen@cqmu.edu.cn (T. Chen).
[1] These authors have contributed equally to this work.

https://doi.org/10.1016/j.bios.2019.111350
Received 21 March 2019; Received in revised form 21 May 2019; Accepted 23 May 2019
Available online 25 May 2019
0956-5663/

masked analytic signal and reduced accuracy of quantitative results (Breault-Turcot et al., 2014; Ye et al., 2015).

Recently, the zwitterionic peptide, formed by alternating negatively charged glutamic acid (E) and positively charged lysine (K) amino acid residues, has received more and more attention owing to its antifouling property. The peptide with hydrophilic groups, such as NH_3^+ and COO^-, tends to form hydrophobicity and helical secondary structures with high surface density via hydrogen bonds and maintains overall charge neutrality (Walker et al., 2018). Moreover, the hydrogen bonds between water and peptide do not destroy the freedom of peptide fragment configuration. Thus, the hydration of zwitterionic polymers may form a comb-like molecular conformation, which provides an another obstacle to biomolecules adsorption (Ziemba et al., 2018). Therefore, zwitterionic peptide is capable of resisting the nonspecific adsorption of charged proteins on the biosensing interface. This unique biological and tunable nature of zwitterionic peptide has made them the most promising potential antifouling biomaterials for biomedical applications (Wang et al., 2018a).

Fiber optic surface plasmon resonance (FO-SPR) biosensor has been increasingly employed in the fields of food safety (Khedri et al., 2018), clinical diagnosis (Lu et al., 2017) and environmental monitor (Caucheteur et al., 2015). In a conventional FO-SPR sensor, an unpolarized light beam travels through an optical fiber covered with Au film on the surface and the reflected light intensity is monitored by a spectrometer. When the frequency of incident light is consistent with the frequency of evanescent waves on metal surfaces, the SPR phenomenon starts to appear and reflected light intensity is significantly reduced (Homola, 2003). Therefore, measuring a variety of target molecules and proteins could be easy to achieve by determining the resonance wavelength or angle shift. FO-SPR is an advanced compact size, low-cost, practical sensing device that offers accurate various features for target analytes (Sharma et al., 2018). And this platform holds great potential as a POCT due to its own advantages. However, traditional FO-SPR biosensors have limited sensitivity for direct detection of biomolecules. Over the years, various metallic nanomaterials have been explored to improve analytical performance of FO-SPR biosensor, such as gold nanoparticles (AuNPs), ZnO nanorods and Fe_2O_3 nanoparticles (Bian et al., 2018; Sharma and Gupta, 2018; Usha et al., 2016). Among these, AuNPs have been extensively applied because of their significant signal amplification ability for FO-SPR. For instance, Lu et al. (2017) proposed a rapid and ease-of-use FO-SPR immunoassay for infliximab measurement utilizing AuNPs for signal enhancement. Qian et al. (2018) reported a FO-SPR sensing strategy for highly sensitive microRNA determination via boronic acid functionalized AuNPs. Daems et al. (2017) designed a competitive inhibition assay for progesterone measurement based on antibody functionalized AuNPs. This enhanced signal is a combined result of greatly increased surface mass accumulation, high dielectric constant of Au particles, and electromagnetic coupling effect related to the distance of AuNPs and Au film (He et al., 2000; Szunerits et al., 2014).

Herein, based aptamer pair and a zwitterionic peptide in homebuild FO-SPR platform, a simple FO-SPR biosensing method was established for highly sensitive PDGF-BB measurement in serum. By taking advantage of zwitterionic peptide and PDGF-BB aptamer functionalized AuNPs, this developed biosensing method shows great potential in clinical application.

2. Materials and methods

2.1. Reagents

The PDGF-binding aptamer and the zwitterionic peptide were synthesized and purified by Sangon Biotechnology Co., Ltd (Shanghai, China). The sequence of the oligonucleotides is 5′-SH-TTTTTTTTCAC AGGCTACGGCACGTAGAGCATCACCATGATCCTGTGT-3' (Gao et al., 2018). The sequence of the peptide is EKEKEKE-PPPPC (purity > 95%) (Nowinski et al., 2012). Recombinant human PDGF-BB and recombinant human VEGF were purchased from PeproTech (Rocky Hill, USA). Tris (2-carboxyethyl) phosphine (TCEP), lysozyme (Lys), uric acid (UA) and bovine serum albumin (BSA) were purchased from Sangon Biotechnology Co., Ltd (Shanghai, China). The human PDGF-BB ELISA kit was obtained from Lianshuo Biological Technology Co., Ltd (Shanghai, China). $HAuCl_4{\cdot}4H_2O$ was purchased from Sinopharm Chem Co., Ltd (Shanghai, China). 6-Mercapto-1-hexanol (MCH) was purchased from Sigma-Aldrich (St. Louis, USA). In addition, other reagents reached the standard of analytical grade. Ultrapure water used in the experiment was prepared by Millipore Milli-Q gradient ultrapure water system (Millipore, USA). The aptamer was dissolved in TE buffer (1 mM EDTA, 10 mM Tris-HCl, pH 8.0) and stored at −20 °C. All the proteins were dissolved in sterile water and diluted with sterile PBS containing 5% trehalose. The serum samples were from the First Affiliated Hospital of Chongqing Medical University. That all experiments were performed in compliance with relevant laws or guidelines.

2.2. Apparatus

A home-built FO-SPR platform and FO probes were used in the biosensor measurement. A fiber cutting device (LDC-400, Vytran, UK) and a sputter coater (Q150T ES Quorum, UK) were used in the FO probe manufacturing. A tungsten halogen lamp (HL-2000-HP, Ocean Optics, USA) and a spectrometer (HR4000, Ocean Optics, USA) were used in the FO-SPR platform construction. The refractive index of NaCl solutions were measured by Abbe refractometer (2WAJ, Shanghai Optic Instrument Plant, China). TEM (H-7500, Hitachi, Japan) was employed to observe the image of AuNPs. UV–visible spectra of aptamer and AuNPs were operated on a spectrophotometer. (UV-2550, Shimadzu, Japan).

2.3. Methods

2.3.1. Preparation of FO probes and FO-SPR platform

The FO probes were fabricated as previously described (Huang et al., 2013). The fiber is multimode optical fiber, and its item No. is FT600UMT (Thorlabs, USA). The numerical aperture of fiber is 0.39. The core and cladding diameter of fiber are 600 μm and 630 μm respectively. The material of core and cladding are silicon and TECS hard polymer respectively. The processing of a FO-SPR biosensor probe contained following stages. Firstly, at one end of the fiber, a 5 mm length of cladding and coating layers on the surface layer of the fiber were removed by chemical etching (pliers and acetone) to ensure the smoothness of the surface of the core. In order to ensure the reflectivity of the core end face, a special fiber cutting device was used to complete the cutting of the core end face. The fiber was finely washed with ethanol and acetone to remove any impurities from the surface that may affect the gold-plating effect. Next, the gold layer was deposited around the bare core of the fiber via thermal evaporation in the vacuum chamber under the pressure of 5×10^{-6} Torr. As a result, a 50 nm thick layer of Au film was covered on the surface of fiber. The adjacent end surface of the fiber was coated with a metal layer about 100 nm thick acted as a mirror. The purpose of mirror was to transmit the incident light back to the spectrometer.

FO-SPR platform was composed of a light source, a plastic cladding multimode optical fiber with quartz core, a spectrometer, a fiber coupler, and a computer with analysis software. Schematic diagram of the FO-SPR biosensing measurement system was shown in Scheme 1B. Incident light beam traveled through an optical fiber covered with Au film on the surface and coupled to the FO-SPR probe through a 2×1 fiber coupler (BIF-4062732-VIS/NIR, USA). Then the FO probe was immersed into the reaction reagent and the unpolarized light was modulated by superficial reaction solutions in the biosensing interface. Moreover, the light was reflected several times on the sensing region of the gold film. Finally, the light was reflected back by the Au layer on the

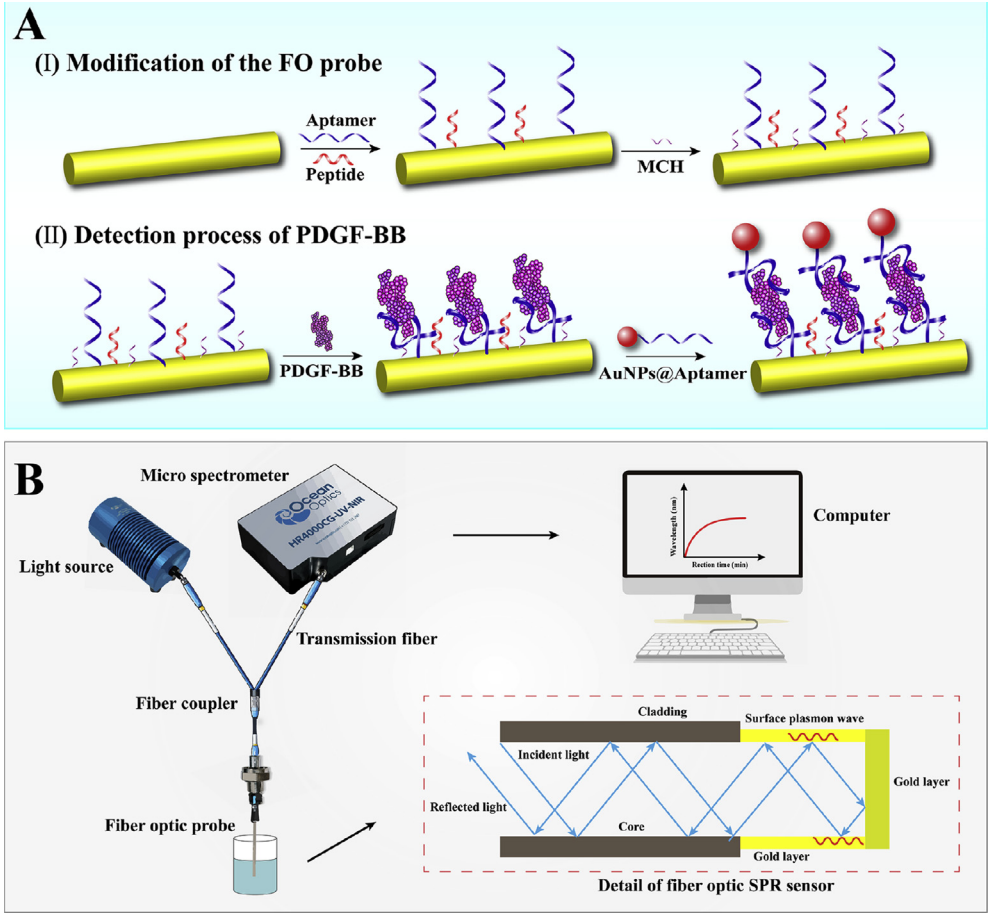

Scheme 1. (**A**) Schematic illustration of PDGF-BB FO-SPR biosensor. (**B**) Schematic diagram of the FO-SPR biosensing detection system.

end surface of the fiber and captured by a fiber optic spectrometer. All data was eventually transferred to the computer.

2.3.2. Preparation of surface functionalized FO probes

The thiolated PDGF binding aptamer and the zwitterionic peptide with amino acid cysteine (C) were immobilized on gold coated optical fibers (FO probes) by the gold-sulfur bond interaction. The process of modification included several steps. In short, the thiol-modified aptamer and the peptide were activated by incubated with 10 mM TCEP in PBS buffer for 1 h at room temperature, and the concentrations of aptamer and peptide were 1 μM and 0.10 mg mL^{-1} respectively. The freshly sputtered FO probes were finely cleaned with ethanol and ultrapure water to ensure modification effect of aptamer and peptide. Then the FO probes were dried by nitrogen gas to avoid contamination, and finally immersed in PBS buffer containing 1 μM aptamer and 0.10 mg mL^{-1} peptide for 24 h at 4 °C. During the process, both the aptamer and peptide were attached onto the surface of FO probes via thiol anchor. Followed washing with ultrapure water, the FO probes were immersed into 1 mM MCH solution for 1 h at room temperature. Considering the ability of MCH in removing the weakly bound aptamers and peptides and blocking the nonspecific binding sites, it was also introduced onto FO probes surfaces via thiol anchor to stabilize peptide monolayer conformation, and further enhance the antifouling capability of peptide SAM surface (Cui et al., 2017). The obtained biosensing interface consisted of recognition elements and antifouling material. The recognition elements were aptamers to respond to the target protein, antifouling material was hydrophobic peptide SAM. After washing with deionized water, FO probes were stored in PBS buffer until further use.

2.3.3. Preparation of AuNPs and aptamer-functionalized AuNPs

AuNPs were prepared by the classic citrate reduction method (Zhu et al., 2014). Briefly, 100 mL of 0.01% tetrachloroauric acid solution was heated to the boiling point. Subsequently 4 mL of 1% trisodium citrate was added quickly with vigorous mechanical stirring to give rise to the formation of gold nanoparticles. Next, the solution continuously heated for 15 min and the color of solution deepened and eventually turned to burgundy red.

Aptamer-functionalized AuNPs were obtained according to previous literature (Wei et al., 2018). First of all, 40 μL of 10 μM thiol-modified aptamer was activated using 4 μL of 10 mM TCEP and 4 μL of 500 mM acetate buffer (pH 5.2) at room temperature for 1 h. Then the aptamer was added into 2 mL of AuNPs solution with gentle stirring for about 24 h to ensure sufficient reaction. After that, 20 μL of 500 mM Tris-acetate buffer (pH 8.2) and 200 μL of 1 M NaCl were successively added to the mixture. Subsequently, the mixture was placed for 24 h at room temperature. Finally, the resulting mixture was centrifuged at 15,000 rpm for 15 min and washed with deionized water. Again, the AuNPs were resuspended in PBS buffer for further use.

2.3.4. FO-SPR biosensor measurement

A bioassay for PDGF-BB determination was implemented according to the following processes. Firstly, the aptamer and peptide modified FO probes were immersed into 1 mL PBS buffer (10 mM) to reach a stable baseline. Then affinity ligands of the aptamer, PDGF-BB, were introduced in the buffer, and were captured by PDGF binding aptamer that immobilized on the surface of FO probes. When the reaction equilibrium was reached, the FO probes were washed with deionized water and PBS gently. Subsequently, the aptamer-functionalized AuNPs were introduced to the surface of FO probes by recognition the captured

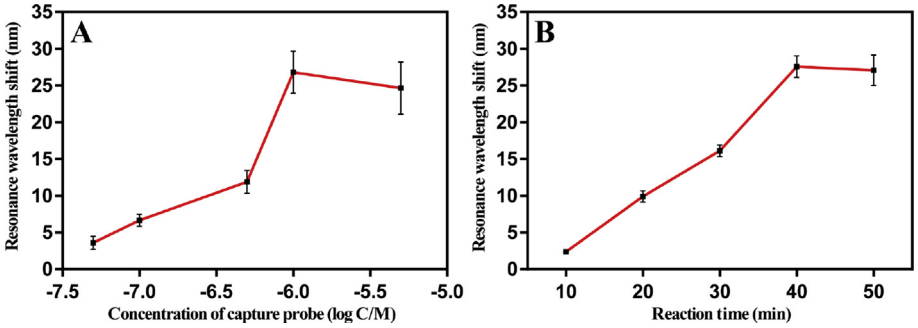

Fig. 1. Optimization of experimental parameters. (**A**) Effect of the concentration of the capture probe on the FO-SPR signal. (**B**) Influence of the reaction time of aptamer and PDGF-BB on the resonance wavelength shifts. The error bars are standard deviations of three repetitive measurements.

PDGF-BB. Finally, the generated signal was recorded for further analysis. All experimental procedures were performed at room temperature.

2.3.5. Data processing

Original spectrograms were recorded using a spectrometer and further transferred to computer. The C++ software was used to monitor experimental process and collect original experimental data, including reaction time, wavelength and reflected light intensity. The MATLAB software was used to analyze original experimental data and plot spectrogram. Each SPR spectrum was the ratio of the 'spectrum of the sample' and the 'air-based reference spectrum'. In a spectrogram, resonance wavelength was determination to the position where the intensity of the reflected light was the lowest. The steepest descent method was performed to determine the location of the minimum spectral reflection. The descent direction was set as a negative gradient since the initial data was in the shorter wavelength region. A large number of iterations were carried out to approach the convergence, and then the location of the resonance wavelength was numerically approximated (Pollet et al., 2009). In the final sensorgram, the SPR resonance wavelength shift was plotted versus reaction time.

3. Results and discussions

3.1. Performance evaluation of the surface unmodified FO-SPR biosensor

The refractive index detection performance of fiber optic biosensor was assessed by monitoring sodium chloride solutions, and the concentration of the sodium chloride solutions corresponded to a different refractive index. Besides, refractive index of the NaCl solutions was related to the resonance wavelength due to the existence of SPR phenomenon. As shown in Fig. S4, the resonance wavelength changed towards longer wavelengths along with the increases of refractive index. There was a good linear relationship between resonance wavelength and refractive index in the range of 1.3327–1.3545 (R^2 = 0.9970). The sensitivity of the FO-SPR biosensor was then calculated to be 2294.50 nm/RIU in this range, which is comparable to the FO-SPR sensor previously reported (Wang et al., 2017).

3.2. Principle of the FO-SPR biosensing strategy

FO-SPR biosensor measurement processes for PDGF-BB is shown in Scheme 1A, which contain two parts, modification of the FO probe and detection process of PDGF-BB. The aptamer and peptide were immobilized onto the FO probe to construct antifouling surfaces by Au–S interaction, then MCH was introduced to stabilize the peptide monolayer. In the presence of target protein, corresponding aptamer captured it specifically, leading to the changes of the effective refractive index near the bioconjugated interface and resonance wavelength redshift. Furthermore, aptamer-functionalized AuNPs were utilized to assemble a bioconjugated complexes near interface of the FO probe for signal amplification. There are two main factors contributing to this signal amplification, distance dependent electromagnetic field coupling and size/mass properties associated with AuNPs. AuNPs with high mass could give rise to a huge variation in refractive index near the bioconjugated sensing surface. The electromagnetic field coupling effect between the AuNPs and propagating plasmons on the Au film surface can further induce signal enhancement (Qian et al., 2018).

A typical sensorgram is shown in Fig. S5. A small resonance wavelength shift signal was observed with only PDGF-BB introduced at 10 min. Subsequently, the aptamer-functionalized AuNPs were introduced to the surface of FO probes at 50 min and the final signal (in red) was greatly amplified. Nevertheless, with the lack of PDGF, only a inappreciable FO-SPR signal (in blue) was monitored even with addition of aptamer-functionalized AuNPs.

3.3. Optimization of the detection conditions

In order to achieve the satisfactory performance of the FO-SPR biosensor, the detection parameters were comprehensively investigated. The aptamer was fixed on the surface of FO probe to act as the affinity receptor of the target protein PDGF-BB. Therefore, the concentration of aptamer is a significant factor for the performance of FO-SPR biosensor. As shown in Fig. 1A, at a given concentration of PDGF-BB (50 pM), the resonance wavelength gradually redshift accompanied by the increase of aptamer concentration from 0.05 μM to 1.0 μM. However, when the concentration of aptamer went beyond 1.0 μM, the signal decreased. High concentration of aptamer immobilized on the gold film might increase steric hindrance for the target protein binding (He et al., 2014). Therefore, the optimal aptamer concentration of 1.0×10^{-6} M was employed in subsequent experiments.

In addition, the reaction time of aptamer and target protein was also crucial in the PDGF-BB detection. As shown in Fig. 1B, the resonance wavelength shift increased as the reaction time was prolonged and approached the maximum after 40 min and kept a plateau. Therefore, the optimal reaction time of target molecule and aptamer was 40 min and that was applied in all further experiments.

3.4. Analytical performance of PDGF detection

The responses of FO-SPR biosensor in the detection of the target protein was examined under the optimal experimental conditions. Time-dependent resonance wavelength shift along with the change of PDGF-BB concentrations were shown in Fig. 2A. The resonance wavelength increasingly redshift with the increase of target protein concentrations in the range of 1–1000 pM. The shift of FO-SPR resonance wavelength varied linearly with the PDGF-BB concentration in the range from 1 to 100 pM (Fig. 2B). The correlation equation was $Y = 0.3451\ X + 4.159$ with $R^2 = 0.985$, where X was the

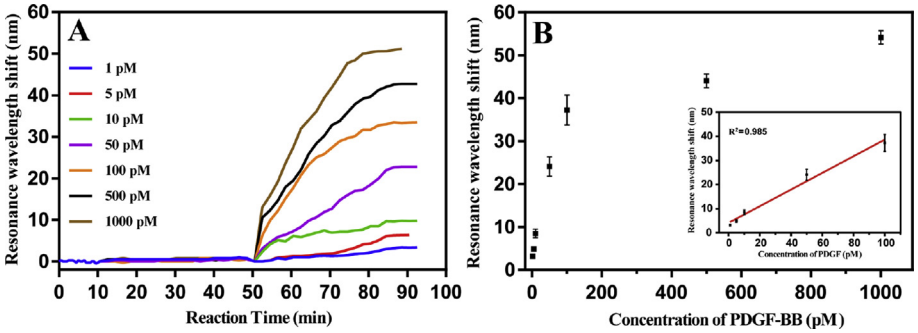

Fig. 2. (**A**) Real-time resonance wavelength responses of the amplified FO-SPR biosensor for PDGF-BB detection. (**B**) Relationship between the resonance wavelength shifts and the target PDGF-BB concentrations. The error bars are standard deviations of three repetitive measurements.

concentration of PDGF-BB and Y was the FO-SPR resonance wavelength shift. Based on the 3σ rule, the limit of detection (LOD) for PDGF-BB was estimated to be 0.35 pM, which is lower than those of the reported aptasensors strategies for PDGF-BB determination (Table S1). Furthermore, in comparison with developed method and others in the detection of proteins based on FO biosensing platform (Table S2), the proposed sandwich strategy achieved high sensitivity for protein measurement. The high sensitivity could be related to the simultaneous combination of the LSPR-SPR effect and the size/mass-material properties of AuNPs for signal amplification (Frasconi et al., 2010). Therefore, this designed FO-SPR biosensor sandwich strategy keeps a greatly potentials for PDGF-BB detection.

3.5. Antifouling property of the FO-SPR biosensor

To investigate the antifouling ability of the self-assembled peptide monolayer interface in preventing nonspecific adsorption, different concentrations of single protein solution were employed as the test media to incubate with FO probes. In order to test the effect of charge repulsion, we chose BSA (with positive electrical charge) and LYS (with negative electrical charge) deliberately. Specifically, the proteins were both dissolved in PBS buffer, and the final mass fraction were 1% and 0.5%, respectively. As shown in Fig. 3, in comparison with FO probes without peptides, the FO probes with peptides showed remarkably more slight resonance wavelength shifts. Therefore, zwitterionic peptide is capable of resisting the nonspecific adsorption of charged proteins on the biosensing interface. (Nowinski et al., 2012).

3.6. Specificity of the FO-SPR biosensor

The specificity of this biosensor was investigated by evaluating with different proteins. As shown in Fig. 4, there were no significant resonance wavelength shifts of the FO-SPR in the presence of nontarget proteins, such as vascular endothelial growth factor (VEGF), bovine serum albumin (BSA), uric acid (UA), lysozyme (LYS). On the contrary, a remarkably increase of resonance wavelength shift was obtained in the presence of PDGF-BB. The results manifested that the FO-SPR biosensing strategy holds high specificity for PDGF-BB detection.

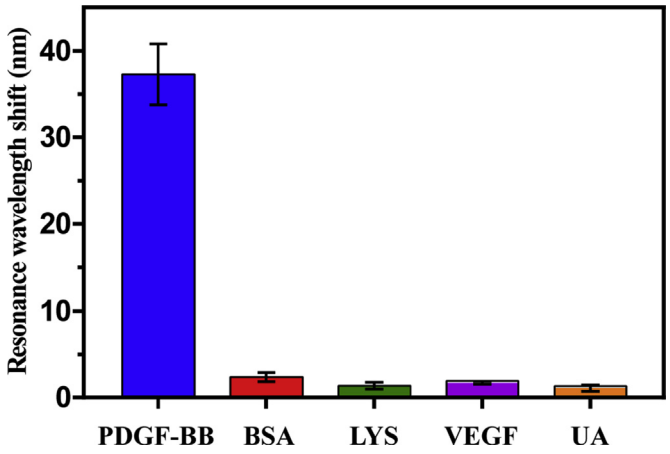

Fig. 4. Resonance wavelength shifts responses to different protein in PBS buffer (concentration of PDGF-BB: 100 pM and others: 1 nm). The error bars are standard deviations of three repetitive measurements.

3.7. Detection of PDGF in human serum

We further evaluated the potential applicability of the FO-SPR biosensor in real sample. Different concentrations of PDGF-BB in 10% (V/V) human serum samples (serum samples were diluted by PBS buffer) were measured, and the results obtained were showed in Table S3. The spiked serum samples were further measured via an ELISA kit and FO-SPR biosensor, and the biosensor detection results were close to that measured with the ELISA kit (Table S4), attributing to the excellent antifouling property of peptides. These results demonstrated the developed FO-SPR biosensing method can detect PDGF-BB in complex biological media, and the home-build FO-SPR biosensing platform might become a pragmatic tool in the field of point-of- care diagnosis.

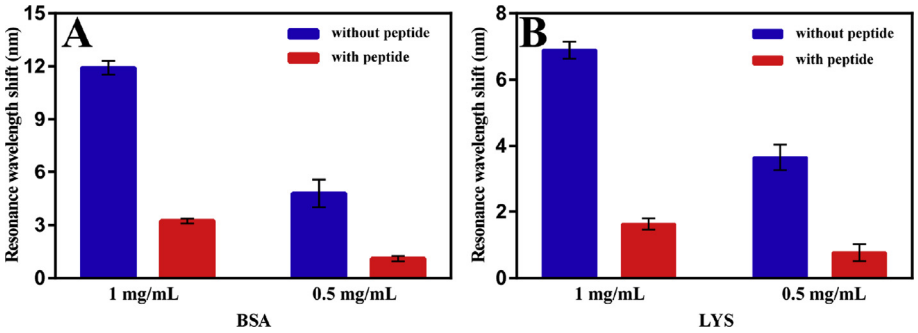

Fig. 3. Resonance wavelength shifts of the FO-SPR biosensor (red cuboids: MCH/Apt-Pep, blue cuboids: MCH/Apt) after incubation in BSA (A) and LYS (B) solution. The error bars are standard deviations of three repetitive measurements. (For interpretation of the references to color in this figure legend, the reader is referred to the Web version of this article.)

4. Conclusions

In summary, a simple, cost-effective and antifouling FO-SPR biosensor was successfully established for highly sensitive detection of PDGF-BB. Significantly, the biosensor was applied for the assay of PDGF-BB in human serum samples, attributing to antifouling ability of the peptide. Therefore, the proposed strategy provides a low-cost and simple platform for label-free and highly sensitive proteins determination in human serum samples, which holds a potential for further application in clinical diagnostics. Nevertheless, sensitivity and antifouling property need to be further improved for this biosensing strategy. Thus, further in-depth studies will focus on the sensitivity enhancement and development of new antifouling materials in FO-SPR biosensor.

Declaration of interests

The authors declare that they have no known competing financial interests or personal relationships that could have appeared to influence the work reported in this paper.

The authors declare the following financial interests/personal relationships which may be considered as potential competing interests:

CRediT authorship contribution statement

Husun Qian: Conceptualization, Methodology, Software, Investigation, Data curation, Writing - original draft. **Yu Huang:** Methodology, Software, Investigation, Project administration, Writing - review & editing. **Xiaolei Duan:** Formal analysis, Software. **Xiaotong Wei:** Conceptualization, Data curation. **Yunpeng Fan:** Resources, Software. **Delu Gan:** Resources, Validation. **Shujun Yue:** Resources, Software. **Wei Cheng:** Supervision, Methodology, Data curation, Project administration.

Acknowledgements

This work was supported by the National Natural Science Foundation of China (No. 81272544 and No. 81873980), Natural Science Foundation of Chongqing (Grant No. cstc2018jcyjAX0718).

Appendix A. Supplementary data

Supplementary data to this article can be found online at https://doi.org/10.1016/j.bios.2019.111350.

References

Bahreyni, A., Tahmasebi, S., Ramezani, M., Alibolandi, M., Danesh, N.M., Abnous, K., Taghdisi, S.M., 2019. Sensor. Actuator. B Chem. 280, 10–15.
Bi, S., Luo, B., Ye, J., Wang, Z., 2014. Biosens. Bioelectron. 62, 208–213.
Bian, S., Lu, J., Delport, F., Vermeire, S., Spasic, D., Lammertyn, J., Gils, A., 2018. Drug Test. Anal. 10 (3), 592–596.
Breault-Turcot, J., Chaurand, P., Masson, J.-F., 2014. Anal. Chem. 86 (19), 9612–9619.
Caucheteur, C., Guo, T., Albert, J., 2015. Anal. Bioanal. Chem. 407 (14), 3883–3897.
Cui, M., Wang, Y., Wang, H., Wu, Y., Luo, X., 2017. Sensor. Actuator. B Chem. 244, 742–749.
Daems, D., Lu, J., Delport, F., Marien, N., Orbie, L., Aernouts, B., Adriaens, I., Huybrechts, T., Saeys, W., Spasic, D., Lammertyn, J., 2017. Anal. Chim. Acta 950, 1–6.
Frasconi, M., Tortolini, C., Botre, F., Mazzei, F., 2010. Anal. Chem. 82 (17), 7335–7342.
Gao, S., Zheng, X., Wu, J., 2018. Biosens. Bioelectron. 102, 57–62.
He, L., Musick, M.D., Nicewarner, S.R., Salinas, F.G., Benkovic, S.J., Natan, M.J., Keating, C.D., 2000. J. Am. Chem. Soc. 122 (38), 9071–9077.
He, P., Liu, L., Qiao, W., Zhang, S., 2014. Chem. Commun. 50 (12), 1481–1484.
Homola, J., 2003. Anal. Bioanal. Chem. 377 (3), 528–539.
Hosaka, K., Yang, Y., Seki, T., Nakamura, M., Andersson, P., Rouhi, P., Yang, X., Jensen, L., Lim, S., Feng, N., 2013. Nat. Commun. 4 (7), 2129.
Huang, Y., Zhang, W., Xie, W., Tang, D., Zhang, H., Du, C., 2013. Sensor. Actuator. B Chem. 186, 199–204.
Jiang, W., Tian, D., Zhang, L., Guo, Q., Cui, Y., Yang, M., 2017. Microchim. Acta. 184 (11), 4375–4381.
Khedri, M., Ramezani, M., Rafatpanah, H., Abnous, K., 2018. Trac. Trends Anal. Chem. 103, 126–136.
Kim, J., Kim, C.-S., Jo, K., Cho, Y.-S., Kim, H.-G., Lee, G.-H., Lee, Y.M., Sohn, E., Kim, J.S., 2015. Biochem. Biophys. Res. Commun. 456 (1), 53–58.
Lu, J., Spasic, D., Delport, F., Van Stappen, T., Detrez, I., Daems, D., Vermeire, S.v., Gils, A., Lammertyn, J., 2017. Anal. Chem. 89 (6), 3664–3671.
Meng, H.-M., Liu, H., Kuai, H., Peng, R., Mo, L., Zhang, X.-B., 2016. Chem. Soc. Rev. 45 (9), 2583–2602.
Nowinski, A.K., Sun, F., White, A.D., Keefe, A.J., Jiang, S., 2012. J. Am. Chem. Soc. 134 (13), 6000–6005.
Pollet, J., Delport, F., Janssen, K.P., Jans, K., Maes, G., Pfeiffer, H., Wevers, M., Lammertyn, J., 2009. Biosens. Bioelectron. 25 (4), 864–869.
Qian, S., Lin, M., Ji, W., Yuan, H., Zhang, Y., Jing, Z., Zhao, J., Masson, J.F., Peng, W., 2018. ACS Sens. 3 (5), 929–935.
Razmi, N., Baradaran, B., Hejazi, M., Hasanzadeh, M., Mosafer, J., Mokhtarzadeh, A., de la Guardia, M., 2018. Biosens. Bioelectron. 113, 58–71.
Sharma, A.K., Pandey, A.K., Kaur, B., 2018. Opt. Fiber Technol. 43, 20–34.
Sharma, S., Gupta, B.D.J.A.O., 2018. Appl. Opt. 57 (36), 10466–10473.
Song, W., Li, H., Liang, H., Qiang, W., Xu, D., 2014. Anal. Chem. 86 (5), 2775–2783.
Szunerits, S., Spadavecchia, J., Boukherroub, R., 2014. Rev. Anal. Chem. 33 (3), 153–164.
Usha, S.P., Shrivastav, A.M., Gupta, B.D., 2016. Biosens. Bioelectron. 85, 986–995.
Walker, J.A.-T., Robinson, K.J., Munro, C., Gengenbach, T., Muller, D.A., Young, P.R., Lua, L.H., Corrie, S.R., 2018. Langmuir.
Wang, W., Mai, Z., Chen, Y., Wang, J., Li, L., Su, Q., Li, X., Hong, X., 2017. Sci. Rep. 7 (1), 16904.
Wang, Y., Cui, M., Jiao, M., Luo, X., 2018a. Anal. Bioanal. Chem. 410 (23), 5871–5878.
Wang, Y.H., Chen, Y.X., Wu, X., Huang, K.J., 2018b. Colloids Surf. B Biointerfaces 172, 407–413.
Wei, X., Duan, X., Zhou, X., Wu, J., Xu, H., Min, X., Ding, S., 2018. Analyst 143 (13), 3134–3140.
Ye, H., Wang, L., Huang, R., Su, R., Liu, B., Qi, W., He, Z., 2015. ACS Appl. Mater. Interfaces 7 (40), 22448–22457.
Ye, S., Zhai, X., Wu, Y., Kuang, S., 2016. Biosens. Bioelectron. 79, 130–135.
Yi, B., Williams Pj Fau - Niewolna, M., Niewolna, M., Fau - Wang, Y., Wang, Y., Fau - Yoneda, T., Yoneda, T., 2002. Cancer Res. 62 (3), 917–923.
Zhang, J.-J., Cao, J.-T., Shi, G.-F., Huang, K.-J., Liu, Y.-M., Ren, S.-W., 2015. Talanta 132, 65–71.
Zhu, D., Yan, Y., Lei, P., Shen, B., Cheng, W., Ju, H., Ding, S., 2014. Anal. Chim. Acta 846, 44–50.
Ziemba, C., Khavkin, M., Priftis, D., Acar, H., Mao, J., Benami, M., Gottlieb, M., Tirrell, M., Kaufman, Y., Herzberg, M., 2018. Langmuir.
Zou, L., Li, R., Zhang, M., Luo, Y., Zhou, N., Wang, J., Ling, L., 2017. Nanoscale 9 (5), 1986–1992.